Title

Circularity in mixed-plastic chemical recycling enabled by variable rates of polydiketoenamine hydrolysis

Journal

Science Advances, 8(29)

ISSN

2375-2548

Authors

Demarteau, Jeremy
Epstein, Alexander R
Christensen, Peter R
et al.

Publication Date

2022-07-22

DOI

10.1126/sciadv.abp8823

Peer reviewed

CHEMISTRY

Circularity in mixed-plastic chemical recycling enabled by variable rates of polydiketoenamine hydrolysis

Jeremy Demarteau[1], Alexander R. Epstein[2], Peter R. Christensen[1], Mark Abubekerov[1], Hai Wang[1], Simon J. Teat[3], Trevor J. Seguin[4], Christopher W. Chan[1], Corinne D. Scown[5,6,7,8], Thomas P. Russell[4,9,10], Jay D. Keasling[5,6,11,12,13], Kristin A. Persson[1,2], Brett A. Helms[1,4,14]*

Footwear, carpet, automotive interiors, and multilayer packaging are examples of products manufactured from several types of polymers whose inextricability poses substantial challenges for recycling at the end of life. Here, we show that chemical circularity in mixed-polymer recycling becomes possible by controlling the rates of depolymerization of polydiketoenamines (PDK) over several orders of magnitude through molecular engineering. Stepwise deconstruction of mixed-PDK composites, laminates, and assemblies is chemospecific, allowing a prescribed subset of monomers, fillers, and additives to be recovered under pristine condition at each stage of the recycling process. We provide a theoretical framework to understand PDK depolymerization via acid-catalyzed hydrolysis and experimentally validate trends predicted for the rate-limiting step. The control achieved by PDK resins in managing chemical and material entropy points to wide-ranging opportunities for pairing circular design with sustainable manufacturing.

INTRODUCTION

Products manufactured from two or more blended, compatibilized, or laminated polymer resins are ubiquitous in municipal waste and present obstacles to chemical recycling because of the difficulty in deconstructing each polymer to their respective monomers for reuse in manufacturing (*1*–*3*). Recycling efforts are further challenged when plastic waste is mixed with metal or glass. In such cases, high-temperature melt filtration becomes necessary to isolate polymers from these solids, which adds considerable cost during the preprocessing of heterogeneous plastic waste (*4*–*6*). The inability to recover valuable chemical and material resources from mixed-polymer and mixed-material products at the end of useful life is both wasteful and unsustainable (*7*–*16*). Furthermore, the accumulation of these waste streams and their leakage into the environment continue to strain global ecosystems (*17*–*23*).

Here, we show that chemospecificity in mixed-polymer recycling is enabled through molecular engineering of polydiketoenamines (PDKs) (*24*, *25*), where fast- and slow-to-depolymerize PDK chemistries incorporated into either mixed-polymer or mixed-material products allow each PDK variant to be selectively deconstructed in space and time simply by varying the depolymerization temperature under acidic conditions (Fig. 1A). PDK resins are deconstructed as solids in the presence of metals and glass, obviating the high-cost melt filtration step required for recycling commodity plastics. At each stage of the thermally controlled recycling process, we recover specific monomers, additives, and fillers from PDK resins in either mixed-PDK blends, laminates, or assemblies that are indistinguishable from the associated primary feedstocks and reusable in closed-loop material life cycles (Fig. 1, B and C). The predictability and control afforded by PDKs in multistage chemical recycling suggest that a common infrastructure may be used to recycle complex products that would normally be considered nonrecyclable. Because specialized plastic recycling infrastructure is capital intensive (*26*), a general process that handles a variety of materials—from polymers and thermosets to composites—could offer economic advantages and even enable recycling in industries that produce durable goods. If implemented, PDK resins could relax a growing number of constraints faced by supply chain managers and product designers when making material choices for circularity to meet their sustainability goals (*27*, *28*) to reduce the need for virgin resin. Pairing recycle-by-design chemistries with customer-focused take-back schemes is also poised to improve industrial material efficiency.

RESULTS

Molecular engineering of triketone monomers yields structurally diverse PDK resins

Mixed-plastic recycling is difficult to achieve with commodity polymers. This is readily evidenced in the chemical depolymerization of three widely used polyesters: poly(ethylene terephthalate) (PET), poly(trimethylene terephthalate) (PTT), and poly(ethylene furanoate) (PEF) (fig. S1A). We performed alkaline hydrolysis of millimeter-sized milled samples of PET from a plastic water bottle, PTT from carpet, and PEF from resin pellets (fig. S1B). All three polyesters depolymerized within 24 hours at 120°C in an aqueous solution of NaOH (20% w/w). We found through ^{1}H nuclear magnetic resonance (NMR) analysis of both the insoluble and soluble components of

[1]The Molecular Foundry, Lawrence Berkeley National Laboratory, Berkeley, CA 94720, USA. [2]Materials Sciences and Engineering, University of California, Berkeley, Berkeley, CA 94720, USA. [3]Advanced Light Source, Lawrence Berkeley National Laboratory, Berkeley, CA 94720, USA. [4]Materials Sciences Division, Lawrence Berkeley National Laboratory, Berkeley, CA 94720, USA. [5]Joint BioEnergy Institute, Emeryville, CA 94608, USA. [6]Biological Systems and Engineering Division, Lawrence Berkeley National Laboratory, Berkeley, CA 94720, USA. [7]Energy Analysis and Environmental Impacts Division, Lawrence Berkeley National Laboratory, Berkeley, CA 94720, USA. [8]Energy and Biosciences Institute, University of California, Berkeley, Berkeley, CA 94720, USA. [9]Polymer Science and Engineering Department, University of Massachusetts, Amherst, MA 01003, USA. [10]Advanced Institute for Materials Research, Tohoku University, Sendai 980-8577, Japan. [11]Department of Chemical and Biomolecular Engineering and Department of Bioengineering, University of California, Berkeley, Berkeley, CA 94720, USA. [12]Center for Synthetic Biochemistry, Institute for Synthetic Biology, Shenzhen Institutes of Advanced Technologies, Shenzhen 518055, China. [13]Novo Nordisk Foundation Center for Biosustainability, Technical University of Denmark, Lyngby, Denmark. [14]Chemical Sciences Division, Lawrence Berkeley National Laboratory, Berkeley, CA 94720, USA.
*Corresponding author. Email: bahelms@lbl.gov

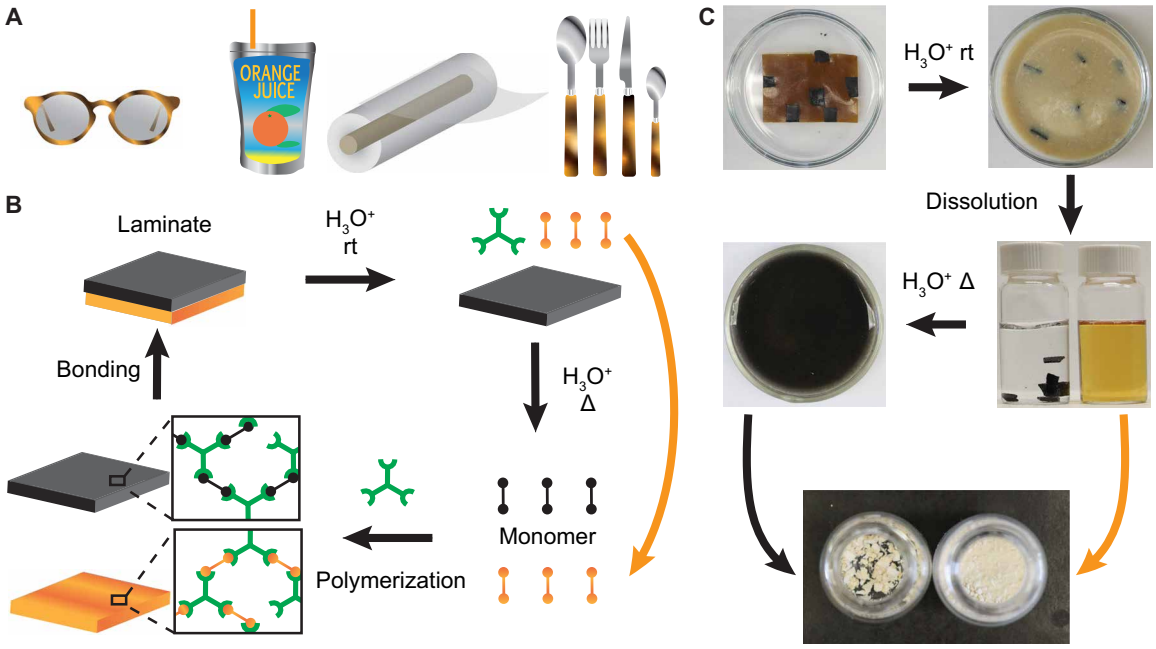

Fig. 1. Closed-loop chemical recycling of mixed-polymer waste. (**A**) Examples of consumer products featuring several polymer resins whose inextricability poses challenges to recycling at the end of life for resource recovery. (**B**) Mixed-polymer recycling can be realized if each polymer was to undergo chemical depolymerization at a different temperature, allowing specific monomers to be recovered in successive stages of the recycling process. These monomers may then be used in secondary polymer resin manufacturing processes to reduce the demand for primary chemical feedstocks. (**C**) Realization of mixed-polymer recycling with polydiketoenamine (PDK) resins, where molecular engineering of diketoenamine polymer bonds enables fine control over polymerization rates in strong acid. Each PDK variant is deconstructed in a chemospecific manner simply by varying the depolymerization temperature.

the reaction mixture that the former constituted terephthalic acid and 2,5-furandicarboxylic acid, while the latter constituted primarily ethylene glycol and trimethylene glycol with trace amounts of both aromatic diacids. To refine diol and diacid monomers for reuse in resin production, separations become necessary and may therefore be prohibitive at manufacturing scale from a cost perspective. Thus, it is an outstanding challenge to efficiently depolymerize mixed-plastic waste into highly refined monomers for circular plastic resin manufacturing when the chemistry of the polymers is similar.

To address outstanding challenges in mixed-plastic recycling, we hypothesized that molecular engineering may provide access to PDK resins with tunable rates of diketoenamine hydrolysis, such that different monomers could be isolated at different stages of a chemical recycling process. PDK resins are synthesized from polytopic triketone and amine monomers via spontaneous "click" polycondensation reactions (*24*, *25*), which proceed under ambient conditions and do not require a promoter. Monomers used in PDK resins share structural similarities with those used to formulate a range of properties in polyurethanes and nylons. The properties of PDK resins might be anticipated to be similar while bridging those of plastics and thermosets because of their dynamic covalent character (*24*, *25*, *29*–*32*). In prior work, we demonstrated that by varying the cross-linking density of PDK resins with flexible and rigid diamines used in polyamides and polyurethanes, we can control tensile strength (stress at break) over a range of 18 to 31 MPa (*25*). This range is similar to that reported for commercially available polyurethanes: 0.6 to 44.1 MPa (*33*). While the formulation science of PDK resins across chemical space remains an active area of research, these early results show that the thermomechanical properties of PDK resins may follow similar design rules as those for nylon and PU.

While the formulation space for tailoring PDK properties is broad, resins formulated with structurally similar triketone monomers depolymerize at similar rates. For example, while changing the carbon chain length in triketone monomers used to synthesize PDK **1** changes their glass transition temperature and other characteristics (Fig. 2), it does not considerably change the rate of their chemical depolymerization to monomer, which is complete in ~12 hours at 25°C or in ~1 hour at 90°C in 5.0 M H_2SO_4 or HCl (*24*). Therefore, to differentiate the rates of PDK depolymerization, we designed PDKs **2** to **4**, which vary in number and placement of heteroatoms relative to the keto functionality in the ring (Fig. 2A); the number of methyl substituents was kept constant, providing the necessary structural similarity to isolate the effects of heteroatoms on hydrolysis rates. Electronegative heteroatoms placed adjacent to a carbonyl affect the basicity and other characteristics of diketoenamines, which we hypothesized could be exploited to alter their susceptibility for hydrolysis and potentially access orthogonal rates of PDK depolymerization in acid. If this were realized, it could enable stepwise recovery of the embodied resources in mixed-PDK and mixed-material waste streams during chemical recycling.

To test this hypothesis, we synthesized PDK resins **1** to **4** from a cohesive group of ditopic triketone monomers **1** to **4** and *tris*(2-aminoethyl)amine (TREN) (Fig. 2A). As evidenced from single-crystal x-ray diffraction (XRD) data (Fig. 2B) and their corresponding chemical structures in Fig. 2A, the preferred tautomer of triketone monomers **2** to **4** features an exocyclic enol, whereas that for triketone **1** features an endocyclic enol. Furthermore, the degree of asymmetry

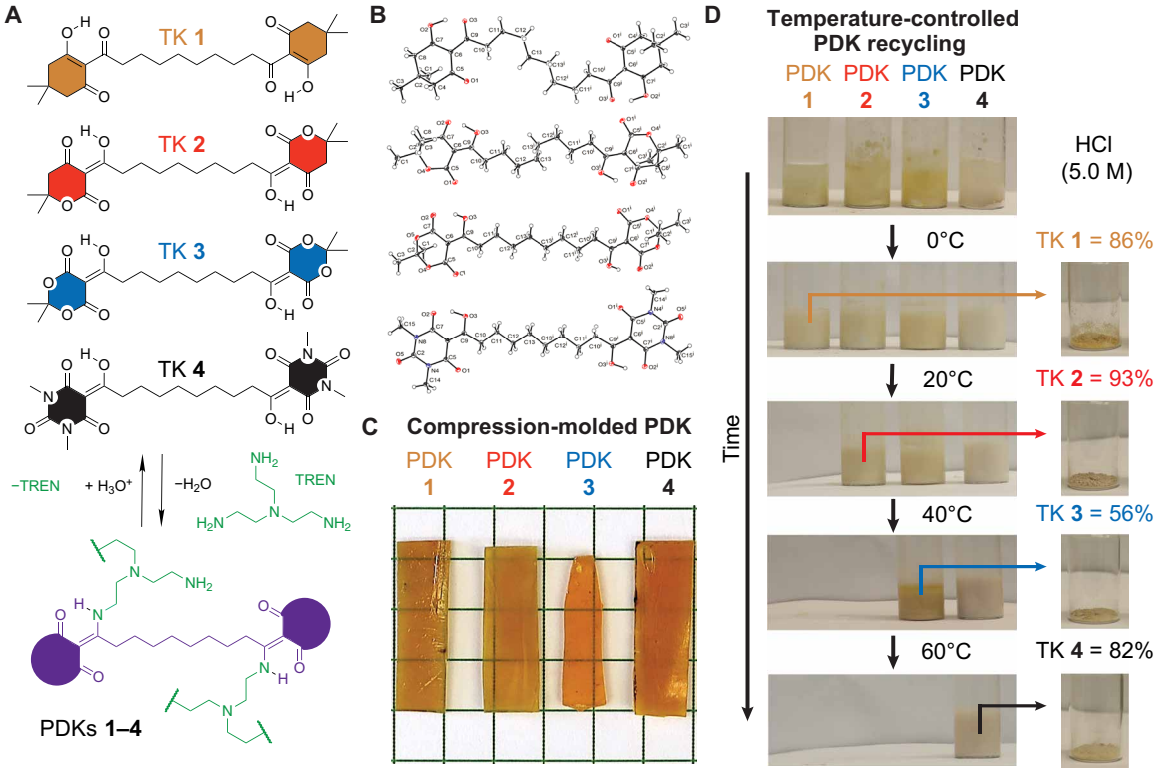

Fig. 2. Molecularly engineered PDKs are depolymerized selectively and iteratively at different temperatures. (**A**) Triketone (TK) monomers **1** to **4** and their use in the chemical synthesis of PDKs **1** to **4** by polycondensation with *tris*(2-aminoethyl)amine (TREN). (**B**) Single-crystal x-ray structures for triketones **1** to **4** show distinctive packing in the solid-state and structure-dependent hydrogen-bond symmetry and preferred tautomer. (**C**) Compression-molded samples of PDKs **1** to **4**. (**D**) Chemospecific recycling of PDKs **1** to **4** to triketone and TREN monomers in 5.0 M HCl at 0°, 20°, 40°, and 60°C. Triketone monomers are recovered in pristine quality from PDKs **1**, **2**, and **4** (figs. S8 to S10) and in high yield. Recovery of triketone **3** was lower because of transformation of some of its chain ends to ß-keto acid, as evidenced by ^{1}H NMR (fig. S11).

in hydrogen bonding highlights notable differences in electronegativity for *O*-centered hydrogen-bond acceptors and donors, with triketones **1** and **4** showing considerable yet opposite asymmetries in hydrogen bonding in comparison to the more symmetric triketone **2** (tables S1 to S5). We also note that while PDK resins **1** to **3** differ only in the heteroatom substitution of cyclic carbons with oxygen, nitrogen substitutions and the additional carbonyl in PDK **4** represent a more divergent chemical motif. Despite these differences, a common and unifying structure for the diketoenamine bond in all PDK resins is evident in XRD data of small-molecule analogs (fig. S2 and table S6) (*24*). PDKs **1** to **4** obtained after ball-mill polymerization were micrometer-sized dispersible powders (fig. S3) and therefore suitable for pelletization or molding (Fig. 2C). Differential scanning calorimetry showed glass transition temperatures (T_g) of 96°, 98°, 104°, and 136°C for PDKs **1** to **4** (figs. S4 to S7), respectively, with only slight variations in tensile storage modulus in the glassy state (1.8 to 2.1 GPa measured at 40°C) or in tensile elastic modulus in the rubbery state (5.3 to 6.9 MPa measured at 180°C) as determined by dynamic mechanical analysis (DMA) (table S7 and figs. S8 to S10). Because of the brittleness of PDK **3**, mechanical properties could not be assessed readily.

PDK variants depolymerize to monomer at different temperatures

To assess the rates of chemical depolymerization of PDKs **1** to **4**, we dispersed resin powders in strong acid (e.g., 5.0 M aqueous HCl) for up to 24 hours at either 0°, 20°, 40°, or 60°C (Fig. 2D). PDK **1** was exclusively depolymerized at 0°C to monomer (86% recovery), whereas PDK **2** was depolymerized at 20°C to monomer with 93% recovery. Elevated temperature was required to depolymerize PDK **3** (56% recovery at 40°C) and PDK **4** (82% recovery at 60°C). Notably, while triketones **1**, **2**, and **4** were recovered from their corresponding PDKs under pristine condition (i.e., indistinguishable from the monomer used in primary resin production), triketone **3** showed evidence of partial transformation to a ß-keto acid in strong acid at elevated temperature (figs. S11 to S15). The poor thermal stability of PDK **3**, along with knowledge of its triketone monomer degradation during hydrolysis, precluded its further consideration for the remainder of this study. In all cases, TREN could be recovered quantitatively from the filtrate after neutralization with a basic ion-exchange resin (*24*). Together, these data confirmed our hypothesis that varying the structure and electronics of the diketoenamine enables variable rates of PDK depolymerization to monomer. The data further suggest that chemically recycling mixtures of resins is possible, permitting the recovery of two or more triketone monomers from TREN in consecutive, yet fully closed loops (Fig. 1).

Torsional strain dictates activation barrier to diketoenamine hydrolysis in strong acid

To understand the contrasting rates of PDK depolymerization to monomer, we carried out density functional theory (DFT) simulations of the reaction coordinates for acid-catalyzed hydrolysis of

small-molecule diketoenamines **1** to **4** (Fig. 3 and figs. S16 to 19), which represent the cleavable bonds in PDKs **1** to **4**, respectively. Hydrolysis proceeds by an addition–elimination mechanism and features transition states corresponding to the addition of water to the acid-activated diketoenamine and the collapse of the tetrahedral hemiaminal to eliminate an alkylammonium and regenerate the triketone (Fig. 3A). We modeled all reactions in an implicit solvent from an initial state consisting of a hydronium ion and a reactive diketoenamine, whose *N*,*N*-dimethylaminoethyl moiety was protonated, as it would be in strong acid. We optimized all molecular geometries using the m06-2X/6-311++G(2df,2p)/SMD level of theory (*34*, *35*) and calculated free energies with the quasi-rigid rotor harmonic oscillator model (table S8) (*36*). We found that protonation of the diketoenamine triggers the formation of an iminium, which rotates out of plane in advance of the addition of water in the rate-limiting step. The out-of-plane rotation is considerably more pronounced in diketoenamines **1** and **2**, whereas diketoenamines **3** and **4** retain a planar structure (fig. S20). Notably, the calculated standard free energies of activation ($\Delta G^{\ddagger}$) for the addition of water to the iminium vary by as much as 13 kJ mol^{-1} between diketoenamine variants (Fig. 3A), and trends are consistent with the observed differences in rates of depolymerization. We also found that differences in $\Delta G^{\ddagger}$ are highly dependent on the energy barrier associated with the rotation of the iminium into the transition state geometry. Specifically, potential energy barriers for rotation (E_{tor}) of the iminium dihedral angle display the same trend as $\Delta G^{\ddagger}$ across diketoenamines **1** to **4** (Fig. 3B).

To experimentally benchmark the theoretical studies of the rate-limiting step for diketoenamine hydrolysis, we measured $\Delta G^{\ddagger}$ for acid-catalyzed hydrolysis of small-molecule diketoenamines **1** to **4**, which we synthesized from the corresponding triketones and *N*,*N*-dimethylethylenediamine. We dissolved diketoenamines **1** to **4** in 5.0 M DCl in D_2O and monitored their hydrolysis to insoluble triketones and soluble amine salts using variable-temperature ^{1}H NMR spectroscopy (figs. S21 to S24). The relative rates of diketoenamine hydrolysis at 20°C vary by over two orders of magnitude, with diketoenamines **1** and **2** hydrolyzing >150 times and >25 times faster than diketoenamine **4**, respectively (Fig. 3C). Furthermore, our calculated values for $\Delta G^{\ddagger}$ for the rate-limiting step in diketoenamine hydrolysis after Eyring analyses of the kinetics

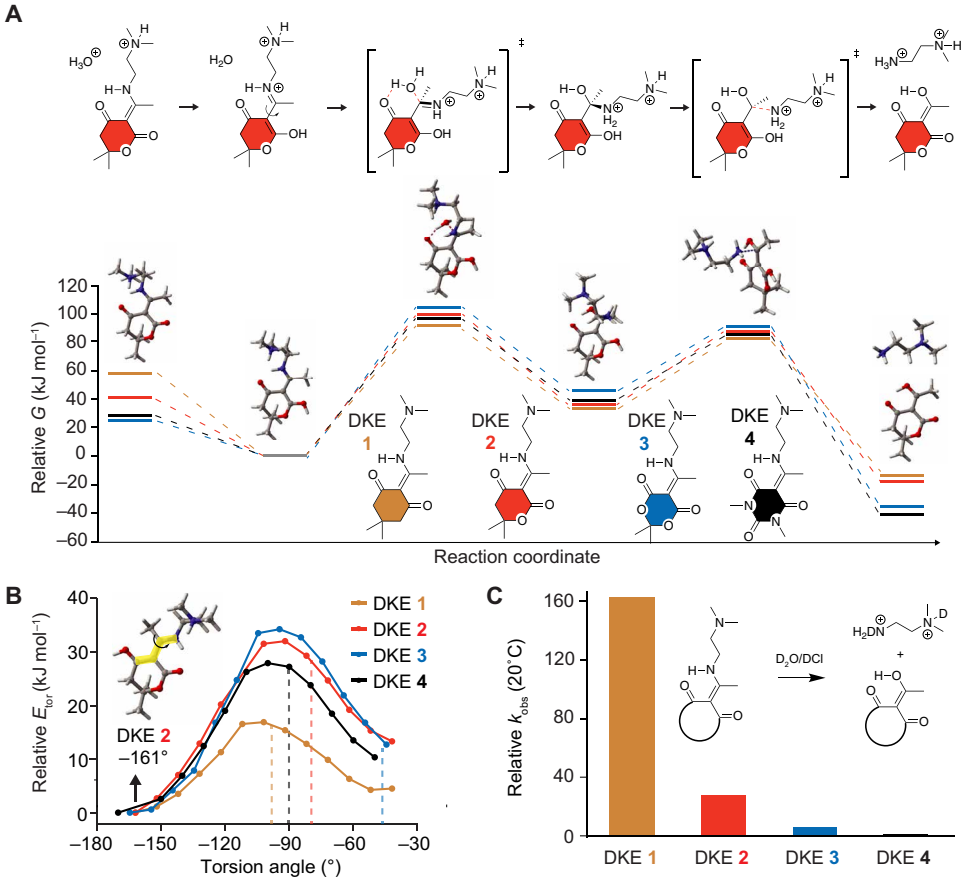

Fig. 3. Molecular basis for the rate-limiting step in PDK hydrolysis. (**A**) Calculated energy landscapes along reaction coordinates for hydrolysis of diketoenamines (DKE) **1** to **4** via an addition-elimination mechanism. Diketoenamines **1** to **4** are studied as surrogates of the bonds in PDK resins **1** to **4** undergoing hydrolysis to triketones in acid. Intermediates along the reaction coordinate are shown for diketoenamine **2**; reaction coordinates for hydrolysis of diketoenamines **1**, **3**, and **4** are given in figs. S16 to S18; reaction path following calculations from the transition states for diketoenamine **2** is shown in fig. S18; free energy values are tabulated in table S9. (**B**) Relative potential energy barriers (E_{tor}) for rotating the iminium out of plane to allow the addition of water in the transition state. Dashed lines indicate the dihedral angle of the transition state. (**C**) Experimentally determined rates of hydrolysis of diketoenamines **1** to **4** in 5.0 M DCl in D_2O at $T = 20$°C; data are normalized to the hydrolysis rate for diketoenamine **4**. Kinetics data at different temperatures and associated Eyring analyses are given in figs. S21 to S24 and table S10.

data agree well with both theoretical determinations (table S10) and the observed temperature-dependent rates of PDK depolymerization as solid or molded resins (Figs. 1 and 2). However, we found that hydrolysis of diketoenamine **4** and, ultimately, depolymerization of PDK **4** were outliers in that their hydrolysis is faster than what is predicted by our DFT simulations. Nitrogen substitutions and the additional carbonyl considerably alter the electronic structure of diketoenamine **4**, leading to a planar ring conformation and a stronger dipole moment. Thus, we expect that the discrepancy between experiment and calculations is due to a more pronounced interaction between diketoenamine **4** and the solvent with high-proton concentration, as compared to the other PDKs. The implicit solvent model used in the calculations does not capture the explicit effects of a hydrogen-bonded solvation structure and possible ionization of the additional carbonyl. Nevertheless, the convergence of computational and experimental data for diketoenamines **1** to **3** provides valid and important insights into the mechanism of diketoenamine hydrolysis and the underlying foundations for the varying rates of hydrolysis by molecular engineering of the diketoenamine bond through targeted heteroatom placement. These modifications unlock orthogonal rates of PDK polymerization, which can be put to use in multipolymer and multimaterial recycling, where there are few options to do so with polymers in use today.

Mixed-polymer and mixed-material recycling enabled by chemospecific PDK deconstruction

To showcase emerging opportunities afforded by molecularly engineered PDKs **1** to **4** in mixed-polymer and mixed-material chemical recycling to monomer, we considered deconstructing an intimate blend of PDKs **1** and **4**, which were prepared separately by ball-milling as fine powders approximately micrometers in size in advance of blending and densification via compression-molding (fig. S3). While blends of thermoplastics are typically melt processed in a twin-screw extruder, blends of PDK vitrimers require alternative measures on account of their dynamic character as cross-linked vitrimers. Notably, while vitrimer powders can be densified by this method, interdiffusion for mixed vitrimer blends is known to be limited when the cross-linking density is high (*37*). Therefore, mixed-PDK blends are expected to be compositionally distinct at the length scales of the powders. This presents an ideal test case for assessing the orthogonality of mixed-PDK depolymerization.

To that end, we mechanically mixed and molded two different PDK resin powders into a microstructured solid bar at 20 kPsi and 140°C for 20 min. We then carried out chemospecific depolymerization of PDKs **1** and **4** in two stages: initially at 20°C endeavoring to depolymerize PDK **1** and then at 60°C to depolymerize PDK **4** (Fig. 4A). After the first stage, we used a simple solid-liquid separation to isolate triketone **1** from intact PDK **4**. After the second stage, we isolated triketone **4** from TREN. Notably, only the prescribed set of monomers was isolated at each stage; we neither observed triketone **4** impurities in triketone **1** recovered in the first stage nor did we observe triketone **1** impurities in triketone **4** recovered in the second stage.

We found that chemospecificity in mixed-PDK recycling with microstructured blends extended to bilayer laminates, where pigments added to one of the resins (in this case, carbon black loaded into PDK **4**) could also be dissociated from the monomers (Fig. 4B). We then considered the deconstruction of trilayer assemblies, e.g., comprising polypropylene (PP) and PET films and featuring PDK **1** as a tie layer between them. This architecture is a crude model for

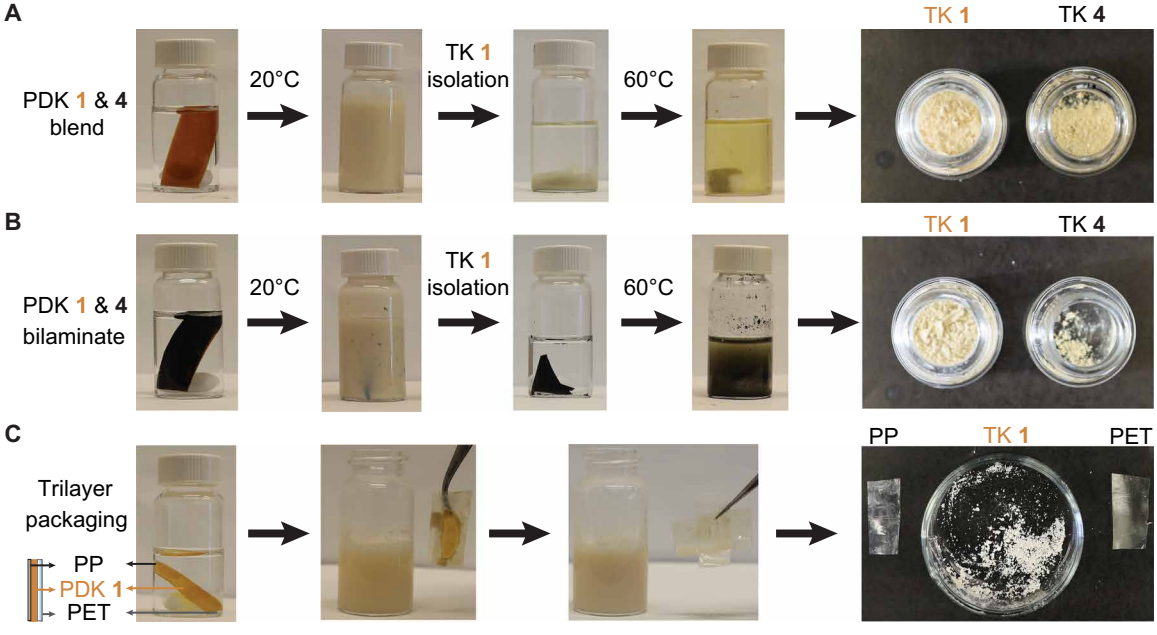

Fig. 4. Chemical circularity in mixed-PDK and mixed-polymer recycling. (**A**) A blend of PDK **1** and **4** resin powders was compression molded into a solid bar sample. At 20°C in strong acid, PDK **1** was chemospecifically depolymerized into triketone monomer **1** and TREN; PDK **4** remained intact and was isolated as a solid. The isolated PDK **4** resin was then depolymerized at 60°C to recover triketone monomer **4** and TREN. (**B**) A bilayer laminate of PDK **1** and carbon black–loaded PDK **4** was chemospecifically deconstructed to prescribed monomers in two stages: initially at 20°C and then at 60°C. (**C**) A trilayer laminate consisting of polypropylene (PP) film and PET film laminated by PDK **1** as a tie layer was deconstructed, enabling PDK recycling as well as PP and PET sorting into homogeneous streams. (A to C) In all cases, recovered monomers showed indistinguishable characteristics from initial monomers, demonstrating chemical circularity in mixed-PDK and mixed-polymer recycling.

multilayer products, in which tie layers complicate the recycling because of difficulties in debonding for later sorting the materials into homogeneous waste streams. Within 24 hours at 20°C, we found that the PDK **1** tie layer was completely depolymerized, despite its low-contact surface area with the acidic depolymerization medium. This allowed both PP and PET films to be separated and sorted (Fig. 4C). We also recovered monomers from PDK **1** without contamination, e.g., from any oligomers or monomers that may have depolymerized from PET in acid.

The orthogonality in PDK depolymerization at different temperatures makes possible the removal or recovery of essentially an endless series of additives compounded into the various PDK resins. As a proof of concept, we compounded a blue pigment in PDK **2** and carbon black in PDK **4** to highlight that de-coloration, and additive dissociation can be conducted concurrently at each stage of the recycling process (Fig. 5A). Despite chemical differences in the two pigments and an increase in number of solid-liquid separations processes, monomer recovery was high: 84% for triketone **2** and 70% for triketone **4**. Both monomers were recovered with indistinguishable properties from those used in primary PDK resin production, thus completing the loop in chemical circularity for mixed polymers and composites (figs. S25 and S26). We provide a guide in table S11 for ensuring chemospecificity and orthogonality in multistage PDK deconstruction via sequential deconstruction in strong acid at different temperatures. To that end, even over extended reaction times at temperatures lower than the prescribed depolymerization temperature, we see little deconstruction: e.g., PDK **4** does not deconstruct to monomer at 40°C for 7 days (fig. S27), whereas PDK resins **1** to **3** readily deconstruct over this time frame at this temperature.

To extend our purview of chemical circularity in mixed-material recycling with PDKs **1** to **4**, we fabricated a bonded assembly comprising metal (stainless steel comprising mainly of Fe with ~12% Cr, ~0.6% C, and the remainder trace elements), glass, and PDKs **1** and **4**; an epoxy resin was used to glue the assembly together (Fig. 5B). This assembly is a crude yet illustrative model for difficult-to-recycle products, from electronics to complex parts integrated into vehicles, aircraft, and buildings (e.g., panels and windows). The challenge in mixed-material recycling is that the conditions used to depolymerize either PDK resin may affect the integrity of the metals and glass through corrosion or etching, respectively. When PDK **1** was depolymerized from the bonded assembly at 20°C in strong acid, the reaction mixture evidenced signs of metal corrosion, even at this low temperature. Despite this, we recovered triketone **1** free from metal and other impurities, as evidenced by both ^{1}H NMR (fig. S28) and inductively coupled plasma optical emission spectrometry (ICP-OES) analysis, which is notable, given the propensity for some triketones to coordinate metals (*38*). After depolymerization PDK **1**, we then deconstructed the remainder of the assembly at 60°C in strong acid, isolating metal from glass and separating triketone **4** from TREN using solid-liquid separations. For recovered triketone **4**, its ^{1}H NMR indicated high purity (fig. S29); however, its slight coloration was tied to 2.79-parts per million (ppm) Fe and 0.19-ppm Cr, as quantified by ICP-OES. While metal contamination in triketone **4** remains lower by nearly two orders of magnitude in comparison to metal contamination of mechanically recycled polymers and slightly lower than virgin resins for commodity plastics (*39*), it can be refined to pristine metal-free quality by recrystallization.

DISCUSSION

The outcomes demonstrated here address outstanding challenges in monomer-to-monomer chemical recycling for both mixed-polymer and mixed-material waste, which require additive- and impurity-tolerant chemical depolymerization and separation processes that are not universally available. Sequential depolymerization of several

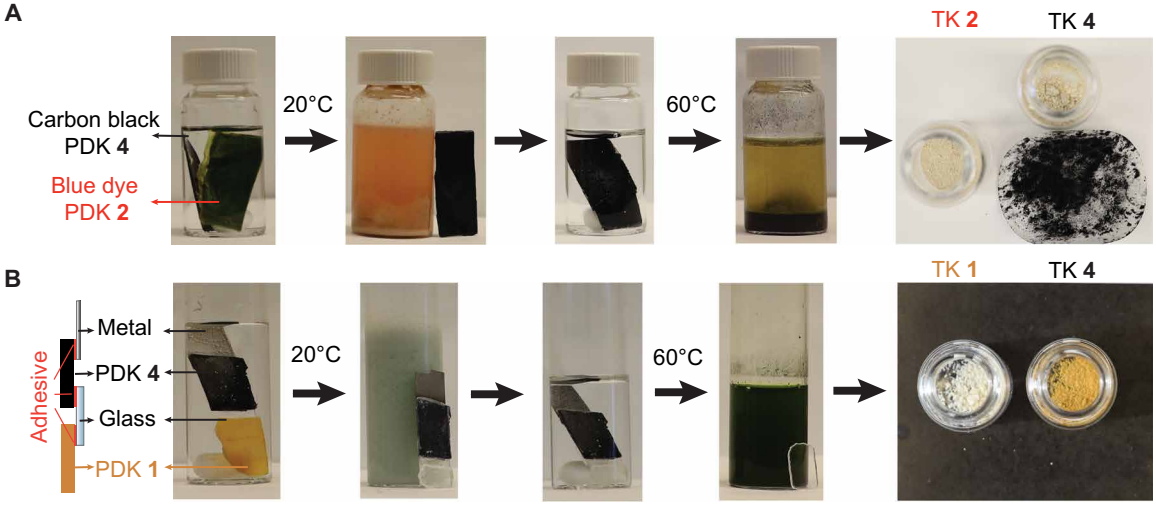

Fig. 5. Chemical circularity in deconstructing multicolor composites and bonded multimaterial assemblies. (**A**) Mixed-PDK composite recycling with de-coloration at each step was demonstrated by first depolymerizing blue dye–loaded PDK **2** at 20°C in strong acid into triketone **2**, TREN, and a blue dye, whose hue is pH dependent. Carbon black–loaded PDK **4** was then retrieved and separately depolymerized at 60°C in strong acid to recover triketone 4 from TREN and carbon black, after filtration (filter shown). (**B**) Mixed-material and mixed-PDK recycling, where compression molded samples of PDK **1** and carbon black–loaded PDK 4 were glued to glass and metal sheets by an epoxy adhesive. PDK **1** was depolymerized at 20°C to recover triketone **1** in pristine condition, which is notable given the contamination of the reaction mixture by metal corrosion. To deconstruct the metal–PDK **4**–glass bonded assembly, the temperature of the strongly acidic solution was raised to 60°C to depolymerize PDK **4** and recover triketone monomer **4**. The presence of an adhesive did not appear to affect the yield or purity of recovered monomers from either PDK **1** or PDK **4**.

polymers in complex mixtures is attractive, allowing reuse of monomer feedstocks, which considerably lowers greenhouse gas emissions in comparison to those generated in primary resin production (*40*–*42*). However, it is rare for each of the polymers in mixed-polymer waste to be depolymerized sequentially to their respective monomers in high yield and purity (fig. S1) (*1*, *2*, *24*, *43*), which, as we show here, becomes possible when using molecularly engineered PDK variants. In this way, PDKs provide an important entry point to managing chemical and material entropy in circular manufacturing systems (*44*).

In early applications, we expect that industries that retain ownership of their assets or implement take-back programs will be most capable of using PDKs in closed-loop recycling. For example, in automotive manufacturing, where polymers and composites comprise nearly 10% of the weight of an average vehicle, chemical circularity could provide a step change in industrial material efficiency as car makers transition to mobility as a service (*5*, *6*). In the long term, we anticipate that collecting and sorting mixed-PDK waste in municipal recycling facilities will benefit from emerging digital barcoding strategies (*45*), which can be used to direct chemical recycling processes efficiently for resource recovery for a more sustainable and circular economy of polymers.

MATERIALS AND METHODS

Materials

5,5-Dimethyl-1,3-cyclohexanedione (dimedone, 95%), 2,2-dimethyl-1,3-dioxane-4,6-dione (Meldrum's acid, 95%), 1,3-dimethylbarbituric acid (>99%), sebacoyl chloride (>95%), 4-(dimethylamino)pyridine (99%), *N*,*N*′-dicyclohexylcarbodiimide (99%), *N*,*N*-dimethylethylenediamine (95%), TREN (96%), magnesium sulfate ($MgSO_4$, anhydrous), sodium hydroxide (NaOH, 98%), potassium carbonate (K_2CO_3, 99%), and hydrochloric acid (HCl) were purchased from Sigma-Aldrich and used as received. Carbon black (Super P Conductive, 99%) was purchased from Alfa Aesar. Bio-based sebacic acid (99%) was purchased from Arkema. Triketone **1** was synthesized as described by us previously (*45*). All solvents—dichloromethane (>99.9%), chloroform (>99.8%), ethyl acetate (>99.8%), hexane (>98.5%), acetone (>99.5%), pyridine (99%), acetonitrile (>99.8%), trifluoroacetic acid (>99.8%), formic acid (98 to 100%), and ethanol (>99.5%)—were purchased from VWR International and used without further purification. *N*,*N*-dimethylacetamide (>99%) was purchased from Sigma-Aldrich and used without further purification. Dihydro-6,6-dimethyl-2*H*-pyran-2,4(3*H*)-dione (*46*), 2-acetyl-5,5-dimethyl-1,3-cyclohexanedione (*24*), 3-acetyl-6,6-dimethyldihydro-2*H*-pyran-2,4(3*H*)-dione (*47*), 5-acetyl-2,2-dimethyl-1,3-dioxane-4,6-dione (*48*), and 5-acetyl-1,3-dimethylpyrimidine-2,4,6(1*H*,3*H*,5*H*)-trione (*49*) were synthesized according to previously reported procedures. Biaxially oriented PP and PET foils were both purchased from Amazon. PET plastic bottle and PTT carpet (100% Triexta) were purchased from a grocery store and widely known home retailer, respectively. PEF pellets were provided by Avantium. Loctite HY 4090 structural hybrid adhesive was purchased from Henkel.

^{1}H and ^{13}C NMR spectroscopy

Analysis was carried out using a Bruker Avance II at 500 and 125 MHz, respectively. Chemical shifts are reported in δ (ppm) relative to the residual solvent peak: (i) $CDCl_3$: 7.26 for ^{1}H, 77.16 for ^{13}C; (ii) d_6–dimethyl sulfoxide: 2.50 for ^{1}H; or (iii) D_2O: 4.8 for ^{1}H NMR for the hydrolysis kinetics in D_2O/DCl 5.0 M. Splitting patterns are designated as s (singlet), d (doublet), t (triplet), q (quartet), and m (multiplet).

Electrospray ionization mass spectrometry

Analysis was carried out using a Bruker microTOF-Q using acetonitrile containing either 0.1% trifluoroacetic acid or 0.1% formic acid as the ionization medium.

Fourier transform infrared spectra

Data were acquired using a PerkinElmer Spectrum One spectrophotometer as an average of 16 scans over 400 to 4000 cm^{-1}.

Single-crystal XRD

Single crystals for triketones **1** to **4** were selected, mounted on Mitegen loops with Paratone oil, and placed in an Oxford Cryosystems Cryostream 800 plus at T = 100 K. Data were collected on beamline 12.2.1 at the Advanced Light Source (Berkeley, CA) with λ = 0.7288 Å using a Bruker D8 diffractometer with a Bruker PHOTONII CPAD detector. Data reduction was performed and corrected for Lorentz and polarization effects using SAINT v8.40a (*50*) and was corrected for absorption effects and other effects using TWINABS 2012/1 (*51*) for triketones **1**, **3**, and **4**, while SADABS v2016/2 (*52*) was used for triketone **2**. Structure solutions were performed by SHELXT (*53*) using the direct method and were refined by least-squares refinement against F^2 by SHELXL (*54*).

Differential scanning calorimetry

Data were acquired using a TA Instruments Q200 Differential Scanning Calorimeter. Samples were heated over a temperature range of either 40° to 220°C (for PDKs **1**, **2**, and **4**) or 40° to 120°C (for PDK **3**) at a rate of 5°C min^{-1} under a N_2 atmosphere. For each sample, data acquisition runs consisted of a heating step, a cooling step, and a second heating step. Glass transition temperatures (T_g) were interpreted and reported from the second heating curve with the exception of PDK **3**; those T_g were interpreted from the first heating curve because of decomposition.

Dynamic mechanical analysis

Data were acquired using a TA Instruments DMA Q800 in tensile mode. All samples were fabricated as rectangular specimens with ~0.5 mm (T) by 5 mm (W) by 20 mm (L). Each sample was tested at a frequency of 1 Hz with a displacement amplitude of 15 μm and a preload force of 0.01 N. Heating ramps of 3°C min^{-1} were applied from 40° to 200°C. The softening temperature was reported as the maximum value of tan δ.

Scanning electron microscopy

Imaging was performed using a Zeiss Gemini Ultra-55 Analytical Field Emission Scanning Electron Microscope with a 5-kV accelerating voltage and using the secondary detector mode. Polymer powders were deposited onto carbon tape affixed to the stainless steel stage in the microscope. Excess polymer was removed using a stream of compressed air, and the sample was sputter coated with gold (thickness ~7 nm) before analysis by scanning electron microscopy (SEM).

Inductively coupled plasma optical emission spectroscopy

Concentrations of Fe and Cr in parts per million in triketones **1** and **4**, chemically recycled using strong acid from mixed-material waste

containing stainless steel, were quantified by ICP-OES 720ES (Varian) equipped with an axial argon torch. For each determination, ~10 mg of triketone was oxidatively digested at ambient temperature in concentrated HNO_3 (~200 µl) for 24 hours and subsequently diluted with MilliQ water to 10 ml in a precision volumetric flask before analysis and comparison to a calibration curve for each element.

Theoretical methods

All DFT calculations were performed using Gaussian 16 (*55*). Pre- and postprocessing of calculation was done using the Python package Pymatgen (*56*). For the reaction pathway free energy calculations, the computational model included the small molecule and one explicit hydronium ion encased in a continuum dielectric medium using the SMD implicit solvent model (*35*). We assumed that proton transfer to and from solvent would proceed rapidly in 5.0 M HCl and thus did not include proton transfer barriers in the calculation. We also assumed facile rotation around sigma bonds and describe the mechanism using the lowest-energy conformer of each reaction step. Our workflow for identifying the lowest-energy conformer for each reaction step is given in the Supplementary Materials.

SUPPLEMENTARY MATERIALS

Supplementary material for this article is available at https://science.org/doi/10.1126/sciadv.abp8823

REFERENCES AND NOTES

1. P. T. Williams, E. A. Williams, Interaction of plastics in mixed-plastics pyrolysis. *Energy Fuel* **13**, 188–196 (1999).
2. M. N. Siddiqui, H. H. Redhwi, Pyrolysis of mixed plastics for the recovery of useful products. *Fuel Process. Technol.* **90**, 545–552 (2009).
3. Z. O. G. Schyns, M. P. Shaver, Mechanical recycling of packaging plastics: A review. *Macromol. Rapid Commun.* **42**, 2000415 (2021).
4. H. S. Park, Y. S. Han, J. H. Park, Massive recycling of waste mobile phones: Pyrolysis, physical treatment, and pyrometallurgical processing of insoluble residue. *ACS Sustain. Chem. Eng.* **7**, 14119–14125 (2019).
5. L. Miller, K. Soulliere, S. Sawyer-Beaulieu, S. Tseng, E. Tam, Challenges and alternatives to plastics recycling in the automotive sector. *Materials* **7**, 5883–5902 (2014).
6. I. Vermeulen, J. V. Caneghem, C. Block, J. Baeyens, C. Vandecasteele, Automotive shredder residue (ASR): Reviewing its production from end-of-life vehicles (ELVs) and its recycling, energy or chemicals' valorization. *J. Hazard. Mater.* **190**, 8–27 (2011).
7. J. Rahimi, M. García, Chemical recycling of waste plastics for new materials production. *Nat. Rev. Chem.* **1**, 46 (2017).
8. J.-B. Zhu, E. M. Watson, J. Tang, E. Y.-X. Chen, A synthetic polymer system with repeatable chemical recyclability. *Science* **360**, 398–403 (2018).
9. G. W. Coates, Y. D. Y. L. Getzler, Chemical recycling to monomer for an ideal, circular polymer economy. *Nat. Rev. Mater.* **5**, 501–516 (2020).
10. I. Vollmer, M. J. F. Jenks, M. C. P. Roelands, R. J. White, T. van Harmelen, P. de Wild, G. P. van der Laan, F. Meirer, J. T. F. Keurentjes, B. M. Weckhuysen, Beyond mechanical recycling: Giving new life to plastic waste. *Angew. Chem. Int. Ed.* **59**, 15402–15423 (2020).
11. M. Häußler, M. Eck, D. Rothauer, S. Mecking, Closed-loop recycling of polyethylene-like materials. *Nature* **590**, 423–427 (2021).
12. H. Jeswani, C. Kruger, M. Russ, M. Horlacher, F. Antony, S. Hann, A. Azapagic, Life cycle environmental impacts of chemical recycling via pyrolysis of mixed plastic waste in comparison with mechanical recycling and energy recovery. *Sci. Total Environ.* **769**, 144483 (2021).
13. B. A. Abel, R. L. Snyder, G. W. Coates, Chemically recyclable thermoplastics from reversible-deactivation polymerization of cyclic acetals. *Science* **373**, 783–789 (2021).
14. M. Mohadjer Beromi, C. R. Kennedy, J. M. Younker, A. E. Carpenter, S. J. Mattler, J. A. Throckmorton, P. J. Chirik, Iron-catalysed synthesis and chemical recycling of telechelic 1,3-enchained oligocyclobutanes. *Nat. Chem.* **13**, 156–162 (2021).
15. D. Sathe, J. Zhou, H. Chen, H. W. Su, W. Xie, T. G. Hsu, B. R. Schrage, T. Smith, C. J. Ziegler, J. Wang, Olefin metathesis-based chemically recyclable polymers enabled by fused-ring monomers. *Nat. Chem.* **13**, 743–750 (2021).
16. L. T. J. Korley, T. H. Epps, B. A. Helms, A. J. Ryan, Toward polymer upcycling-adding value and tackling circularity. *Science* **373**, 66–69 (2021).
17. J. R. Jambeck, R. Geyer, C. Wilcox, T. R. Siegler, M. Perryman, A. Andrady, R. Narayan, K. L. Law, Plastic waste inputs from land into the ocean. *Science* **347**, 768–771 (2015).
18. R. Geyer, J. R. Jambeck, K. L. Law, Production, use, and fate of all plastics ever made. *Sci. Adv.* **3**, e1700782 (2017).
19. D. E. MacArthur, Beyond plastic waste. *Science* **358**, 843 (2017).
20. J. B. Lamb, B. L. Willis, E. A. Fiorenza, C. S. Couch, R. Howard, D. N. Rader, J. D. True, L. A. Kelly, A. Ahmad, J. Jompa, C. D. Harvell, Plastic waste associated with disease on coral reefs. *Science* **359**, 460–462 (2018).
21. S. B. Borrelle, J. Ringma, K. L. Law, C. C. Monnahan, L. Lebreton, A. McGivern, E. Murphy, J. Jambeck, G. H. Leonard, M. A. Hilleary, M. Eriksen, H. P. Possingham, H. De Frond, L. R. Gerber, B. Polidoro, A. Tahir, M. Bernard, N. Mallos, M. Barnes, C. M. Rochman, Predicted growth in plastic waste exceeds efforts to mitigate plastic pollution. *Science* **369**, 1515–1518 (2020).
22. A. Stubbins, K. L. Law, S. E. Munoz, T. S. Bianchi, L. Zhu, Plastics in the Earth system. *Science* **373**, 51–55 (2021).
23. M. MacLeod, H. P. H. Arp, M. B. Tekman, A. Jahnke, The global threat from plastic pollution. *Science* **373**, 61–65 (2021).
24. P. R. Christensen, A. M. Scheuermann, K. E. Loeffler, B. A. Helms, Closed-loop recycling of plastics enabled by dynamic covalent diketoenamine bonds. *Nat. Chem.* **11**, 442–448 (2019).
25. C. He, P. R. Christensen, T. J. Seguin, E. A. Dailing, B. M. Wood, R. K. Walde, K. A. Persson, T. P. Russell, B. A. Helms, Conformational entropy as a means to control the behavior of poly(diketoenamine) vitrimers in and out of equilibrium. *Angew. Chem. Int. Ed.* **59**, 735–739 (2020).
26. T. W. Walker, N. Frelka, Z. Shen, A. K. Chew, J. Banick, S. Grey, M. S. Kim, J. A. Dumesic, R. C. Van Lehn, G. W. Huber, Recycling of multilayer plastic packaging materials by solvent-targeted recovery and precipitation. *Sci. Adv.* **6**, eaba7599 (2020).
27. Ellen MacArthur Foundation. The new plastics economy: Rethinking the future of plastics & catalysing action (Ellen MacArthur, 2017); www.ellenmacarthurfoundation.org/publications/the-new-plastics-economy-rethinking-the-future-of-plastics-catalysing-action.
28. S. Billiet, S. R. Trenor, 100th anniversary of macromolecular science viewpoint: Needs for plastics packaging circularity. *ACS Macro Lett.* **9**, 1376–1390 (2020).
29. S. J. Rowan, S. J. Cantrill, G. R. L. Cousins, J. K. M. Sanders, J. F. Stoddart, Dynamic covalent chemistry. *Angew. Chem. Int. Ed.* **41**, 899–952 (2002).
30. D. Montarnal, M. Capelot, F. Tournilhac, L. Leibler, Silica-like malleable materials from permanent organic networks. *Science* **334**, 965–968 (2011).
31. W. Denissen, J. M. Winne, F. E. Du Prez, Vitrimers: Permanent organic networks with glass-like fluidity. *Chem. Sci.* **7**, 30–38 (2016).
32. Y. Jin, Z. Lei, P. Taynton, S. Huang, W. Zhang, Malleable and recyclable thermosets: The next generation of plastics. *Matter* **1**, 1456–1493 (2019).
33. J. Datta, P. Kasprzyk, Thermoplastic polyurethanes derived from petrochemical or renewable resources: A comprehensive review. *Polym. Eng. Sci.* **58**, E14–E35 (2018).
34. Y. Zhao, D. G. Truhlar, The M06 suite of density functionals for main group thermochemistry, thermochemical kinetics, noncovalent interactions, excited states, and transition elements: Two new functionals and systematic testing of four M06-class functionals and 12 other functionals. *Theor. Chem. Acc.* **120**, 215–241 (2008).
35. A. V. Marenich, C. J. Cramer, D. G. Truhlar, Universal solvation model based on solute electron density and on a continuum model of the solvent defined by the bulk dielectric constant and atomic surface tensions. *J. Phys. Chem. B* **113**, 6378–6396 (2009).
36. S. Grimme, Supramolecular binding thermodynamics by dispersion-corrected density functional theory. *Chem. A Eur. J.* **18**, 9955–9964 (2012).
37. C. He, S. Shi, X. Wu, T. P. Russell, D. Wang, Atomic force microscopy nanomechanical mapping visualizes interfacial broadening between networks due to chemical exchange reactions. *J. Am. Chem. Soc.* **140**, 6793–6796 (2018).
38. V. Rusanov, A. Ahmedova, M. Mitewa, A Mössbauer study on iron(II) complex of 2-acetyl-1,3-indandione – Spin-crossover or structural changes. *Eur. J. Chem.* **5**, 176–180 (2014).
39. M. K. Eriksen, K. Pivnenko, M. E. Olsson, T. F. Astrup, Contamination in plastic recycling: Influence of metals on the quality of reprocessed plastic. *Waste Manag.* **79**, 595–606 (2018).
40. N. Vora, P. R. Christensen, J. Demarteau, N. R. Baral, J. D. Keasling, B. A. Helms, C. D. Scown, Leveling the cost and carbon footprint of circular polymers that are chemically recycled to monomer. *Sci. Adv.* **7**, eabf0187 (2021).
41. J. Demarteau, N. Vora, J. D. Keasling, B. A. Helms, C. D. Scown, Lower-cost, lower-carbon production of circular polydiketoenamine plastics. *ACS Sustainable Chem. Eng.* **10**, 2740–2749 (2022).
42. S. R. Nicholson, N. A. Rorrer, A. C. Carpenter, G. T. Beckham, Manufacturing energy and greenhouse gas emissions associated with plastics consumption. *Joule* **5**, 673–686 (2021).
43. C. Jehanno, J. Demarteau, D. Mantione, M. C. Arno, F. Ruiperez, J. L. Hedrick, A. P. Dove, H. Sardon, Selective chemical upcycling of mixed plastics guided by a thermally stable organocatalyst. *Angew. Chem. Int. Ed.* **60**, 6710–6717 (2021).
44. K. Kuemmerer, J. H. Clark, V. G. Zuin, Rethinking chemistry for a circular economy. *Science* **367**, 369–370 (2020).

45. J. Paben, https://resource-recycling.com/plastics/2020/01/03/companies-embrace-invisible-barcode-to-aid-in-sorting/ (2020).
46. X. Xu, X. Xu, P. Y. Zavalij, M. P. Doyle, Dirhodium(II)-catalyzed formal [3+2+1]-annulation of azomethine imines with two molecules of a diazo ketone. *Chem. Commun.* **49**, 2762–2764 (2013).
47. S. Gelin, B. Chantegrel, C. Deshayes, Synthesis of some 4-carboxy-3- and 5-(2-hydroxyalkyl) pyrazole lactone derivatives. *J. Heterocycl. Chem.* **19**, 989–992 (1982).
48. J. H. Sahner, H. Sucipto, S. C. Wenzel, M. Groh, R. W. Hartmann, R. Mueller, Advanced mutasynthesis studies on the natural α-pyrone antibiotic myxopyronin from myxococcus fulvus. *Chembiochem* **16**, 946–953 (2015).
49. J. Figueiredo, J. L. Serrano, M. Soares, S. Ferreira, F. C. Domingues, P. Almeida, S. Silvestre, 5-Hydrazinylethylidenepyrimidines effective against multidrug-resistant Acinetobacter baumannii: Synthesis and in vitro biological evaluation of antibacterial, radical scavenging and cytotoxic activities. *Eur. J. Pharm. Sci.* **137**, 104964 (2019).
50. SAINT Software for CCD Diffractometers, Bruker AXS Inc., Madison, WI. (2014).
51. G. M. Sheldrick, TWINABS, Bruker Analytical X-ray Systems, Inc., Madison, WI. (2000).
52. G. M. Sheldrick, SADABS, Bruker Analytical X-ray Systems, Inc., Madison, WI. (2000).
53. G. M. Sheldrick, A short history of SHELX. *Acta Crystallogr. A* **64**, 112–122 (2008).
54. G. M. Sheldrick, Crystal structure refinement with SHELXL. *Acta Crystallogr. Sect. C Struct. Chem.* **71**, 3–8 (2015).
55. M. J. Frisch, G. W. Trucks, H. B. Schlegel, G. E. Scuseria, M. A. Robb, J. R. Cheeseman, G. Scalmani, V. Barone, G. A. Petersson, H. Nakatsuji, X. Li, M. Caricato, A. V. Marenich, J. Bloino, B. G. Janesko, R. Gomperts, B. Mennucci, H. P. Hratchian, J. V. Ortiz, A. F. Izmaylov, J. L. Sonnenberg, D. Williams-Young, F. Ding, F. Lipparini, F. Egidi, J. Goings, B. Peng, A. Petrone, T. Henderson, D. Ranasinghe, V. G. Zakrzewski, J. Gao, N. Rega, G. Zheng, W. Liang, M. Hada, M. Ehara, K. Toyota, R. Fukuda, J. Hasegawa, M. Ishida, T. Nakajima, Y. Honda, O. Kitao, H. Nakai, T. Vreven, K. Throssell, J. A. Montgomery Jr., J. E. Peralta, F. Ogliaro, M. J. Bearpark, J. J. Heyd, E. N. Brothers, K. N. Kudin, V. N. Staroverov, T. A. Keith, R. Kobayashi, J. Normand, K. Raghavachari, A. P. Rendell, J. C. Burant, S. S. Iyengar, J. Tomasi, M. Cossi, J.M. Millam, M. Klene, C. Adamo, R. Cammi, J. W. Ochterski, R. L. Martin, K. Morokuma, O. Farkas, J. B. Foresman, D. J. Fox, *Gaussian 16*, Revision A.03, Gaussian Inc., Wallingford CT, (2016).
56. S. P. Ong, W. D. Richards, A. Jain, G. Hautier, M. Kocher, S. Cholia, D. Gunter, V. L. Chevrier, K. A. Persson, G. Ceder, Python materials genomics (pymatgen): A robust, open-source python library for materials analysis. *Comp. Mat. Sci.* **68**, 314–319 (2013).
57. P. Pracht, F. Bohle, S. Grimme, Automated exploration of the low-energy chemical space with fast quantum chemical methods. *Phys. Chem. Chem. Phys.* **22**, 7169–7192 (2020).
58. N. Mardirossian, M. Head-Gordon, How accurate are the Minnesota density functionals for noncovalent interactions, isomerization energies, thermochemistry, and barrier heights involving molecules composed of main-group elements? *J. Chem. Theory Comput.* **12**, 4303–4325 (2016).
59. H. Eyring, The activated complex in chemical reactions. *J. Chem. Phys.* **3**, 107–115 (1935).

Acknowledgments: We thank T. Mattox and R. Dziedzic for ICP-OES and SEM, respectively. We also thank A. Zapata and A. Mariano for performing the preliminary studies. **Funding:** The technical scope of work associated with the chemistry development was supported by the Laboratory Directed Research and Development Program of Lawrence Berkeley National Laboratory under U.S. Department of Energy (DOE) contract no. DE-AC02-05CH11231. For mixed-polymer and mixed-material recycling, we acknowledge support from the U.S. DOE Bioenergy Technologies Office award number 1916-1597. This research used the Savio computational cluster resource provided by the Berkeley Research Computing program at the University of California, Berkeley (supported by the UC Berkeley chancellor, vice chancellor for research, and chief information officer). We also acknowledge grant no. NIH S10OD023532 for additional computational resources. A.R.E. was supported by the National Science Foundation Graduate Research Fellowship under grant no. DGE 1752814. Portions of this work, including monomer synthesis and characterization, were carried out as a User Project at the Molecular Foundry, which is supported by the Office of Science, Office of Basic Energy Sciences, of the U.S. DOE under contract no. DE-AC02-05CH11231. Single-crystal x-ray characterization was carried out at the Advanced Light Source, which is a DOE Office of Science User Facility operating under the same contract. **Author contributions:** B.A.H. designed and directed the study and wrote the manuscript. J.D., P.R.C., H.W., and C.W.C. synthesized and characterized the monomers and polymers. J.D. compounded and processed the polymers, performed thermomechanical characterization, and conducted the recycling experiments. M.A. performed small-molecule hydrolysis kinetics experiments. S.J.T. conducted single-crystal x-ray crystallography and analyzed the results. K.A.P. directed and A.R.E. and T.J.S. designed and executed the computational studies. All coauthors participated in the data analysis and interpretation. **Competing interests:** B.A.H. and P.R.C. are inventors on the U.S. provisional patent application 62/587,148 submitted by Lawrence Berkeley National Laboratory that covers PDKs, as well as aspects of their use and recovery. P.R.C. has a financial interest in FLO Materials. J.D.K. has a financial interest in Amyris, Lygos, Demetrix, Napigen, Maple Bio, Apertor Labs, Berkeley Yeast, Ansa Biotechnologies, and Zero Acre Farms. B.A.H., J.D.K., and C.D.S. have a financial interest in Cyklos Materials. The other authors declare that they have no other competing interests. **Data and materials availability:** All data needed to evaluate the conclusions in the paper are present in the paper and/or the Supplementary Materials. Materials can be provided by the Lawrence Berkeley National Laboratory pending scientific review and a completed material transfer agreement. Requests for materials should be submitted to ipo@lbl.gov.

Submitted 4 March 2022
Accepted 7 June 2022
Published 20 July 2022
10.1126/sciadv.abp8823